Structural and Multidisciplinary Optimization manuscript No.
(will be inserted by the editor)

Craig S. Long · Philip W. Loveday · Albert A. Groenwold

Effects of planar element formulation and numerical integration order on checkerboard material layouts

Received: date / Revised: date

Abstract The effects of selected planar finite element formulations, and their associated integration schemes, on the stiffness of a checkerboard material layout are investigated. Standard 4-node bilinear elements, 8- and 9-node quadratic elements, as well as 4-node elements with drilling degrees of freedom are considered. Integration schemes evaluated include popular Gauss quadrature rules, as well as modified 5- and 8-point integration schemes. It is shown that, although checkerboarding may be slightly alleviated when using elements with drilling degrees of freedom, the homogenized checkerboard stiffness is identical to that of standard bilinear elements. This is significant since elements with drilling degrees of freedom are derived from an 8-node parent element. We do however demonstrate that modified reduced integration schemes, applied to quadratic elements, effectively reduce the stiffness of a checkerboard material layout. Furthermore, the proposed schemes effectively suppress spurious zero energy modes which may occur on the element level in topology optimization.

Keywords checkerboard · homogenization · reduced integration · drilling degrees of freedom

C.S. Long
Sensor Science & Technology, CSIR Material Science & Manufacturing, Box 395, Pretoria, South Africa, 0001.
Tel.: +27-12-8412498
E-mail: clong@csir.co.za

P.W. Loveday
Sensor Science & Technology, CSIR Material Science & Manufacturing, Box 395, Pretoria, South Africa, 0001.
Tel.: +27-12-8414296
E-mail: ploveday@csir.co.za

A.A. Groenwold
Department of Mechanical and Mechatronic Engineering, University of Stellenbosch, Matieland, South Africa, 7602.
Tel.: +27-21-8084243
E-mail: albertg@sun.ac.za

1 Introduction

Topology optimization has seen a resurgence in popularity in recent times, largely credited to the paper of Bendsøe and Kikuchi (1988). This increased research interest has led to many significant advances, and has seen the use of topology optimization in a number of applications and fields. Examples include minimum compliance problems (against which most new procedures and theories are benchmarked), see for example Bendsøe (1989); Zhou and Rozvany (1991), vibration problems considered by, for instance, Pedersen (2000); Díaz and Kikuchi (1992), compliant mechanism design with contributions by, among others, Sigmund (1997); Bruns and Tortorelli (2001) and multiphysics problems, see Sigmund (2001a,b).

It was however accepted relatively early on that there are several numerical issues which need to be carefully dealt with in order to achieve sensible results, for example see Sigmund and Petersson (1998) for a review. One of the numerical issues that has received significant attention is the problem of checkerboarding. Checkerboarding is characterised by a significant part of the material layout forming a checkerboard pattern. That is, if the finite element method is employed and elemental densities are graphically represented on a finite element mesh, the resulting pattern is reminiscent of a checkerboard.

It is pertinent at this stage to emphasise that topology optimization is a challenging global optimization problem. It should therefore be qualified that, although it is instructive to study the mechanics of checkerboard layouts, the severity of checkerboarding in a topology optimization environment is dependant on a number of factors, including optimization algorithm type and settings (such as step limit or starting point), objective function (checkerboarding is less prevalent in compliant mechanism design than minimum compliance problems), as well as problem discretization and whether or not continuation methods are applied. Furthermore, there have been numerous schemes suggested to eliminate checker-

boarding from a design generated using topology optimization. Examples include works by Poulsen (2002a,b) as well as many of the restriction methods. These schemes naturally also have a significant effect on the checkerboarding severity.

The checkerboarding problem was studied in detail by especially Jog and Haber (1996) and Díaz and Sigmund (1995). By interpreting the layout problem as a mixed variational problem in density and displacement, Jog and Haber attribute this problem to a violation of the Babuska-Brezzi or LBB condition. Unfortunately, as reported by Díaz and Sigmund (1995), the conditions under which the standard Babuska-Brezzi arguments are applied to mixed variational problems are not met by the layout optimization problem, see also Bendsøe (1995).

A different approach was adopted by Díaz and Sigmund (1995). They suggested that the pattens can be explained on the basis of local behaviour. They showed that numerical approximations introduced by the finite element method may, under certain circumstances, cause material arranged in a checkerboard fashion to appear artificially stiff. Under these conditions a local arrangement in a checkerboard-like fashion appears to be locally stiffer than any other arrangement of the two constitute materials with the same volume.

In essence, they concluded that since quadratic Q9 elements are 'softer' than Q4 elements, they are less likely to checkerboard. However, the numerical stability of higher order elements (such as Q8 or Q9) comes at a price. They are numerically more expensive than lower order (Q4) elements. Nevertheless, with the advent of ever increasing computing power, this additional expense may become less significant in future. It therefore remains of interest to study the use of higher order elements to alleviate checkerboarding in topology optimization problems. The work of Díaz and Sigmund is built upon here, by exploring the use of reduced integration schemes in higher order elements in order to further reduce the stiffness of a checkerboard patch of elements.

In the earlier days of the development of the finite element method, numerical integration schemes attracted significant attention (e.g. see Dovey (1974); Zienkiewicz et al (1971); Irons (1971); Gupta and Mohraz (1972)), possibly due to the limitations of the computing devices available at the time.

Reduced integration schemes are numerically less expensive than higher order schemes. This saving in computational effort on the element level comes at the expense of integration accuracy. However, the induced integration error is often on higher-order terms which, more often than not, actually enhances finite element accuracy. In summary, reduced integration may be able to simultaneously reduce cost, reduce accuracy in the evaluation of integration expressions, and increase the accuracy of the finite element analysis. This principle was recently successfully applied by Long and Groenwold (2004), who applied modified reduced quadratures to quadratic Q8 and Q9 elements.

Since planar elements with drilling degrees of freedom are based on a quadratic 'parent element', and because it is well known that quadratic elements are less susceptible to checkerboarding than standard bilinear elements, the stiffness of a checkerboard arrangement of elements with drilling degrees of freedom is of interest.

Our paper is constructed as follows: In Section 2 the modified numerical integration schemes employed in this study are briefly described. Section 3 presents a very brief discussion of element formulations with drilling degrees of freedom. The theory used by Díaz and Sigmund to estimate the stiffness of a checkerboard patch is summarised in Section 4. In Section 5 the numerical results of employing reduced integration in evaluating elements with drilling degrees of freedom, as well as higher order elements such as Q8 and Q9, are presented. Finally, conclusions are drawn in Section 6.

2 Reduced modified quadrature integration rules

Reduced integration is frequently used in evaluating the element stiffness matrix of quadratically interpolated finite elements. Reduced integration 'softens' these element, thereby increasing accuracy, albeit at the possible introduction of spurious zero energy modes on the element level. To effectively suppress zero energy modes usually associated with reduced integration schemes in elements employing quadratic interpolation fields, two modified quadratures have recently been employed by Long and Groenwold (2004). As compared to fully integrated elements, the new rules enhance element accuracy due to the introduction of soft, higher-order deformation modes. For completeness, and because these schemes are not widely know, some details regarding the schemes employed are briefly presented here. For further details, the reader is referred to Dovey (1974) or Long and Groenwold (2004).

2.1 Numerical integration schemes

The numerical integration schemes presented in this section are based on those originally proposed by Dovey (1974). Consider the area integral given by

$$I \;=\; \int_{-1}^{1}\int_{-1}^{1} F\,(r,s)\;\,\mathrm{d}r\,\mathrm{d}s, \tag{1}$$

where $F(r,s)$ is any polynomial function of r and s. Any polynomial expression of two variables can be expressed in the form

$$F\,(r,s) \;=\; \sum_{i,j} A_{ij} r^i s^j. \tag{2}$$

No limits are placed on the summation indices i and j as any arbitrary polynomial is being considered. Let any N-point numerical integration rule be written as

$$I^* \;=\; \sum_{n=1}^{N} W_n F\left(r_n, s_n\right), \tag{3}$$

where I^* represents the numerical approximation to I. Integration point n is given by (r_n, s_n) and the associated weight is given as W_n.

Each term of (2) may be trivially integrated as follows:

$$\int_{-1}^{1}\int_{-1}^{1} A_{ij} r^i s^j \;\mathrm{d}r\mathrm{d}s \;=\; \begin{cases} \frac{2^2 A_{ij}}{(i+1)(j+1)} & i,j \text{ both even} \\ 0 & \text{otherwise} \end{cases} \tag{4}$$

Based on this exact integral, a number of numerical approximations may be derived with leading error terms related to ever higher exponents.

2.2 A five-point rule

The 5-point rule is depicted in Figure 1(a). Due to symmetry, the weights W_α are identical. The rule is indicated by

$$I^* \;=\; W_0 F(0,0) + W_\alpha F(\pm\alpha, \pm\alpha). \tag{5}$$

The second term of (5) indicates four points when all combinations of positive and negative signs are taken. Now, combining (2) and (3), comparing with (4) and grouping terms including A_{00}, A_{20} and A_{02} and disregarding the centre weight (refer to Long and Groenwold (2004) for details) leads to

$$\alpha \;=\; 1/\sqrt{3};\;\; W_\alpha \;=\; 1 \;\text{ and }\; W_0 \;=\; 0, \tag{6}$$

which is identical to the 2×2 Gaussian product rule. However, the center point may be retained by selecting a value for W_0 and computing W_α and α. The scheme is now defined by

$$W_\alpha = 1 - W_0/4, \tag{7}$$

$$\alpha = \left(\frac{1}{3W_\alpha}\right)^{\frac{1}{2}}. \tag{8}$$

It was shown by Long and Groenwold (2004) that it is preferable if W_0 is chosen such that $0 \leq W_0 \leq \frac{8}{3}$.

2.3 An eight-point rule

The 8-point rule is depicted in Figure 1(b). The rule is described by

$$I^* \;=\; W_\alpha F(\pm\alpha, \pm\alpha) + W_\beta \left[F(\pm\beta, 0) + F(0, \pm\beta)\right]. \tag{9}$$

The four equations associated with A_{00}, (A_{02} and A_{20}), A_{22} and (A_{04} and A_{40}) may be satisfied simultaneously and the solution is

$$\alpha \;=\; \sqrt{7/9};\;\; W_\alpha \;=\; 9/49;\;\; \beta \;=\; \sqrt{7/15};\;\; W_\beta \;=\; 40/49. \tag{10}$$

This rule gives similar order of accuracy as the 3×3 Gaussian rule. A scheme of lower accuracy is defined by

$$W_\alpha = 1 - W_\beta, \tag{11}$$

$$\alpha = \left(\frac{1}{9W_\alpha}\right)^{\frac{1}{4}}, \tag{12}$$

$$\beta = \left(\frac{2/3 - 2W_\alpha\alpha^2}{W_\beta}\right)^{\frac{1}{2}}. \tag{13}$$

In this case both α and β are restricted to be between 0 and 1. This implies that W_β be chosen such that $0 < W_\beta < \frac{8}{9}$.

3 Elements with drilling degrees of freedom

In this section, a very brief account of formulations of membrane elements with drilling degrees of freedom is presented. These membrane elements account for in-plane rotations based on a continuum mechanics definition of rotation. The approach relies on a variational formulation employing an independent rotation field, as presented by Hughes and Brezzi (1989). It utilizes the skew-symmetric part of the stress tensor as a Lagrange multiplier to enforce equality of independent rotations and the skew-symmetric part of the displacement gradient in a weak sense. The stress tensor is therefore not *a priori* assumed to be symmetric.

Hughes and Brezzi show that a displacement-based functional can be derived by eliminating the skew-symmetric part of stress from a mixed-type functional. Employing a matrix notation similar to that in Zienkiewicz and Taylor (1991), the result is the modified functional

$$\begin{aligned} \mathit{\Pi}_{\mathrm{m}}^{\mathrm{Q4}\gamma}(\boldsymbol{u}_{\mathrm{m}}, \theta_z) = \frac{1}{2}\int_V \boldsymbol{\epsilon}_{\mathrm{m}}{}^T \boldsymbol{C}_{\mathrm{m}} \boldsymbol{\epsilon}_{\mathrm{m}} \mathrm{d}V \\ + \frac{1}{2}\gamma \int_V (\omega_{xy} - \theta_z)^2 \mathrm{d}V - \int_V \boldsymbol{u}_{\mathrm{m}}{}^T \boldsymbol{f} \mathrm{d}V, \end{aligned} \tag{14}$$

where ω_{xy} is the rotational part of the displacement gradient, given by

$$\omega_{xy} = \frac{1}{2}\left(\frac{\partial u}{\partial y} - \frac{\partial v}{\partial x}\right). \tag{15}$$

In the foregoing, $\boldsymbol{\epsilon}_{\mathrm{m}}$ represents the membrane strains, $\boldsymbol{C}_{\mathrm{m}}$ the membrane constitutive matrix, $\boldsymbol{u}_{\mathrm{m}}$ denotes the in-plane membrane displacement field $[u, v]$ and $\boldsymbol{f}$ the body forces.

The independent rotations θ_z are interpolated using standard bilinear functions, while the in-plane displacement approximation is taken as an Allman-type interpolation, refer to Allman (1988).

In matrix form the first term of $\mathit{\Pi}_{\mathrm{m}}^{\mathrm{Q4}\gamma}$ can be shown to reduce to

$$\tilde{\boldsymbol{k}}_{\mathrm{m}}^{\mathrm{Q4}\gamma} \;=\; t\int_A \left[\boldsymbol{B}_{\mathrm{m}}^{\mathrm{Q4}\gamma} \;\; \boldsymbol{G}_{\mathrm{m}}^{\mathrm{Q4}\gamma}\right]^T \boldsymbol{C}_m \left[\boldsymbol{B}_{\mathrm{m}}^{\mathrm{Q4}\gamma} \;\; \boldsymbol{G}_{\mathrm{m}}^{\mathrm{Q4}\gamma}\right] \mathrm{d}A, \tag{16}$$

where $\tilde{\boldsymbol{k}}_{\mathrm{m}}^{\mathrm{Q4}\gamma}$ is a 12×12 matrix, t is the constant element thickness, and $\boldsymbol{C}_m$ is the constitutive matrix. The penalty term, in matrix form, corresponding to the second term of $\mathit{\Pi}_{\mathrm{m}}^{\mathrm{Q4}\gamma}$ is derived as

$$\boldsymbol{p}_{\mathrm{m}}^{\gamma} \;=\; \gamma\int_A \begin{Bmatrix} \boldsymbol{b}_{\mathrm{m}}^{\mathrm{Q4}\gamma} \\ \boldsymbol{g}_{\mathrm{m}}^{\mathrm{Q4}\gamma} \end{Bmatrix} \left[\boldsymbol{b}_{\mathrm{m}}^{\mathrm{Q4}\gamma} \;\; \boldsymbol{g}_{\mathrm{m}}^{\mathrm{Q4}\gamma}\right] \mathrm{d}A, \tag{17}$$

where $\gamma = \bar{\gamma}G,$ (18)

with G the shear modulus and $\bar{\gamma}$ an adjustable parameter, see Long et al (2006). The element stiffness matrix therefore becomes

$$\boldsymbol{k}_{\mathrm{m}}^{\mathrm{Q4}\gamma} = \tilde{\boldsymbol{k}}_{\mathrm{m}}^{\mathrm{Q4}\gamma} + \boldsymbol{p}_{\mathrm{m}}^{\gamma}. \tag{19}$$

$\boldsymbol{p}_{\mathrm{m}}^{\gamma}$ is integrated by a single point Gaussian quadrature. By fully integrating $\tilde{\boldsymbol{k}}_{\mathrm{m}}^{\mathrm{Q4}\gamma}$ and combining with $\boldsymbol{p}_{\mathrm{m}}^{\gamma}$, spurious zero energy modes are prevented, as demonstrated by Ibrahimbegovic et al (1990). The same holds if a modified 8-point quadrature, or 5-point rule (see Geyer and Groenwold (2003)), are employed to integrate $\tilde{\boldsymbol{k}}_{\mathrm{m}}^{\mathrm{Q4}\gamma}$. The forms of $\boldsymbol{B}_{\mathrm{m}}^{\mathrm{Q4}\gamma}$, $\boldsymbol{G}_{\mathrm{m}}^{\mathrm{Q4}\gamma}$, $\boldsymbol{b}_{\mathrm{m}}^{\mathrm{Q4}\gamma}$ and $\boldsymbol{g}_{\mathrm{m}}^{\mathrm{Q4}\gamma}$ can be found in, for example, Ibrahimbegovic et al (1990).

4 Stiffness of a checkerboard patch of elements

In this section the essential theory and results of Díaz and Sigmund (1995) are briefly summarised. Since much of the work presented in this section is based on their work, and in order to ensure continuity for those readers familiar with the work of Díaz and Sigmund, their notation is used here. The section concludes with the main results from the paper by Díaz and Sigmund.

4.1 Effective properties of a checkerboard

Following the procedure set out by Díaz and Sigmund, it is now demonstrated how the effective properties of a 'black-and-white' checkerboard patch of finite elements are computed. This represents a unit base cell Y which is divided into four equal quadrants Y^i such that $E = E^-$ in $Y^1 \cup Y^3$ and $E = E^+$ in $Y^2 \cup Y^4$, as shown in Figure 2.

The homogenized stiffness tensor is computed using the well-known homogenization formulae by integration over the base cell area as:

$$\bar{E}_{ijkl} = \int_Y \left\{E_{ijkl} - E_{ijpq}\epsilon_{pq}^*[\chi^{(kl)}]\right\} \mathrm{d}y, \tag{20}$$

where the $Y-$periodic test fields $\chi_p^{(kl)}$ are found as the solution to the equilibrium equations

$$\int_Y E_{ijkl}\left\{\epsilon_{pq}^*[\chi^{(kl)}] - \epsilon_{pq}^{0^{(kl)}}\right\}\frac{\partial v_i}{\partial y_j}\mathrm{d}y = 0, \tag{21}$$

for all $v \in V^h$, and $k, l = 1, 2$. For details consult Bendsøe and Sigmund (2003); Díaz and Sigmund (1995); Hassani and Hinton (1998a,b,c).

The finite element space V^h contains the same shape functions as those used to approximate the displacement field, defining

$$V^h = \{v(y) \in R^2 : v(y) = N_\alpha(y)v_\alpha^i, \quad \text{if } y \in Y^i,\ i = 1, \ldots, 4\}, \tag{22}$$

and where in the unit base cell, $v(0, y_2) = v(1, y_2)$ and $v(y_1, 0) = v(y_2, 1)$. The effective material tensor, given in (20) can be computed after solving (21) using three linearly independent test strains $\epsilon_{pq}^{0^{(kl)}}$, as discussed in for example Bendsøe and Sigmund (2003); Hassani and Hinton (1998a,b,c); Sigmund (1994).

In their paper, Díaz and Sigmund (1995) find solutions to (20) and (21) using analytical integration of the finite element discretization. For an undistorted mesh of elements, this is equivalent to using full numerical integration, i.e. a 4 point Gauss quadrature for standard 4 noded elements and a 9 point scheme for 9 node elements.

They also present the optimal strain energy density w^* for a known strain field $\bar{\epsilon}$ and average density $\rho = 1/2$ using: (*i*) rank 2 materials, (*ii*) materials with a base cell described by a rectangular hole, as well as (*iii*) SIMP parameterizations, see Figure 3. They then compare these values to the strain energy density calculated using a patch of 4 square elements, as depicted in Figure 2 with the same average density and applied strain field.

In particular, for rank 2 materials, it can be shown (see Díaz and Sigmund (1995) and Jog et al (1993)) that the optimal strain energy density for fixed strain $\bar{\epsilon}$ and density $\rho = 1/2$ is given by

$$w^*_{\mathrm{Rank2}}(\bar{\epsilon}) = \frac{1}{2}\max_{a^e \in X_\rho, \rho^e = 1/2} \bar{E}_{\mathrm{Rank2}}(a)\bar{\epsilon}\cdot\bar{\epsilon}, \tag{23}$$

where

$$X_\rho = \left\{a \in R^2 :\ a_1 + a_2 - a_1a_2 = \rho,\ 0 \le a_1, a_2 \le 1\right\}, \tag{24}$$

and $\bar{E}_{\text{Rank2}}$ is the effective property tensor of the Rank 2 material and the a's are as depicted in Figure 3(b). For a void weak material ($E^- = 0$), $w^*_{\text{Rank2}}(\bar{\epsilon})$ may be expressed analytically. This result is compared to

$$w^*_{\text{Q4}}(\bar{\epsilon}) = \frac{1}{2}\bar{E}_{\text{Q4}}\bar{\epsilon}\cdot\bar{\epsilon}, \tag{25}$$

and

$$w^*_{\text{Q9}}(\bar{\epsilon}) = \frac{1}{2}\bar{E}_{\text{Q9}}\bar{\epsilon}\cdot\bar{\epsilon}, \tag{26}$$

where $\bar{E}_{\text{Q4}}$ and $\bar{E}_{\text{Q9}}$ are, respectively, the effective constitutive tensor of the 'black-and-white' patch of Q4 and Q9 elements, as depicted in Figure 2.

Similarly, for $\rho = 1/2$, the optimal strain energy density for a microstructure with a base cell described by a rectangular hole is given by

$$w^*_{\text{RHole}}(\bar{\epsilon}) = \frac{1}{2}\max_{a^e\in X,\rho^e=1/2}\bar{E}_{\text{RHole}}(a)\bar{\epsilon}\cdot\bar{\epsilon}, \tag{27}$$

and for the SIMP material model,

$$w^*_{\text{SIMP}}(\bar{\epsilon}) = \frac{1}{2}\bar{E}_{\text{SIMP}}(\rho)\bar{\epsilon}\cdot\bar{\epsilon} = \frac{1}{2}\left(\frac{1}{2}\right)^p E^+\bar{\epsilon}\cdot\bar{\epsilon}, \tag{28}$$

where $\bar{E}_{\text{RHole}}$ and $\bar{E}_{\text{SIMP}}$ are the associated constitutive tensors. Given the preceding, the following relationships can be proven:

- For rank 2 layered materials (denoted Rank 2),

$$w^*_{\text{Q4}}(\bar{\epsilon}) \geq w^*_{\text{Rank 2}}(\bar{\epsilon}), \text{ and} \tag{29}$$

$$w^*_{\text{Q9}}(\bar{\epsilon}) < w^*_{\text{Rank 2}}(\bar{\epsilon}). \tag{30}$$

- For a square cell with rectangular hole (denoted RHole),

$$w^*_{\text{Q4}}(\bar{\epsilon}) > w^*_{\text{RHole}}(\bar{\epsilon}), \text{ while} \tag{31}$$

$$w^*_{\text{Q9}}(\bar{\epsilon}) < w^*_{\text{RHole}}(\bar{\epsilon}). \tag{32}$$

- For SIMP material model (denoted SIMP),

$$w^*_{\text{Q4}}(\bar{\epsilon}) = w^*_{\text{SIMP}}(\bar{\epsilon}), \text{ for } p = 1, \tag{33}$$

$$w^*_{\text{Q4}}(\bar{\epsilon}) > w^*_{\text{SIMP}}(\bar{\epsilon}), \text{ for } p > 1, \tag{34}$$

$$w^*_{\text{Q9}}(\bar{\epsilon}) < w^*_{\text{SIMP}}(\bar{\epsilon}), \text{ for } p < p^*_1(\nu), \text{ and} \tag{35}$$

$$w^*_{\text{Q9}}(\bar{\epsilon}) > w^*_{\text{SIMP}}(\bar{\epsilon}), \text{ for } p > p^*_2(\nu), \text{ where} \tag{36}$$

$$p^*_1(\nu) = \frac{\log\left(22/(6-5\nu)\right)}{\log(2)}, \text{ and} \tag{37}$$

$$p^*_2(\nu) = \frac{\log\left(2(6-5\nu)\right)}{\log(2)}. \tag{38}$$

Díaz and Sigmund suggest that checkerboarding is likely to occur if the strain energy density, based on the effective material tensor of a checkerboard patch of elements (e.g. $\bar{E}_{\text{Q4}}$, $\bar{E}_{\text{Q9}}$), is greater than that based on the effective material tensor of the relevant material parameterization (e.g. $\bar{E}_{\text{Rank2}}$, $\bar{E}_{\text{RHole}}$ or $\bar{E}_{\text{SIMP}}$). These relations can therefore be used to, not only explain why checkerboarding occurs, but also in the case of the SIMP material model, to recommend a suitable penalty parameter p.

5 Numerical results

In this section, selected numerical results are presented. Firstly, the effect of finite element formulation on the local test field χ is explored qualitatively. Next, effective material properties of a checkerboard patch of elements are computed, employing various elements making use of different integration schemes. These effective properties are then used to compute strain energy densities for prescribed straining conditions. Finally, for the SIMP material model, the effects of integration scheme on the bounds of penalty parameter p^*_1 and p^*_2 are investigated.

The following elements are considered in this study:

- *Q4*, a standard 4-node displacement based element.
- *Q4X*, a 4-node element with drilling degrees of freedom, based on the variational formulation presented in Section 3.
- *Q8*, the serendipity 8-node element.
- *Q9*, the Lagrange 9-node element.

The integration schemes evaluated are listed below:

- *4-point Gauss-Legendre scheme*, which is standard for evaluating Q4 elements and exact for undistorted elements. It is also commonly used to evaluate Q8 elements, although it leads to a (normally non-communicable) spurious mode on the element level.
- *5-point scheme*, with varying center weight W_0, see Section 2.2.
- *8-point scheme* with varying weight W_β, see Section 2.3.
- *9-point Gauss-Legendre scheme*, which is the standard 3×3 scheme used to evaluate Q9 element matrices and is also commonly used for Q8 elements.

5.1 Effect of element formulation on local χ field

The solution to the cell problem (21) with Q4 elements has been shown to be extremely simple. The periodic deformation subjected to constant test strain is such that the strain in the patch is constant. That is to say,

$$\epsilon^*[\chi^{(kl)}] = 0. \tag{39}$$

To illustrate this, the χ field for a patch of Q4 elements subjected to a constant prestrain $\bar{\epsilon}_{11} = \bar{\epsilon}_{22} = 1$, and $\bar{\epsilon}_{12} = 0$, is depicted in Figure 4(a).

It is now investigated whether the additional straining modes, associated with Q4X elements, result in non-constant patch strains when subjected to similar test strains. These elements are based on an 8-node parent element employing quadratic Allman-type shape functions as outlined in Section 3. The side nodes are 'condensed' to the corner nodes and related to corner nodal rotations. Q4X elements, therefore possess 3 degrees of freedom per node in total, i.e. 2 in-plane translations and an in-plane rotation.

Unfortunately, as with Q4 elements, only constant patch strains result for Q4X elements. This can be attributed to the fact that, in the solution of the cell problem, the rotational degrees of freedom are not activated by any of the test strains, and therefore neither are the higher order straining modes. The resulting local χ field is thus identical to that of Q4, as depicted in Figure 4(a).

In previous work, Long et al (2003) have shown that Q4X elements do in fact yield slightly different results in terms of checkerboarding than Q4 elements. This is probably due to the fact that for realistic problems with complex strain fields, the skew-symmetric part of the displacement gradient becomes non-zero. Under these circumstances Q4X appears to be less stiff than standard Q4 elements, tending to effectively suppress the formation of large areas of checkerboard material layout. To illustrate, Figure 5(a) depicts the optimal topology of the MBB beam employing Q4 elements and a ramping strategy to increase the penalty parameter p linearly from 1 to 3 in 34 iterations, whereafter it is held at $p = 3$ for a further 16 iterations after which the solution is terminated. Figure 5(b) depicts the results employing the same strategy, but this time employing Q4X elements. Clearly, the severity of checkerboarding is significantly reduced compared to the results employing Q4 elements.

However, in the limit of mesh refinement only constant strains are experienced, and under these circumstances (fine meshes) more checkerboarding is expected. Numerical experiments have supported this conjecture. There is therefore no guarantee that Q4X elements will not checkerboard, especially when fine meshes are employed. Having said that, elements with drilling degrees of freedom have been shown to be useful in topology optimization applications for other applications, e.g. see Long et al (2003, 2005, 2004). Q4X elements are also more accurate and more robust than standard Q4 elements, at only a slight increase in numerical expense.

The local χ fields for Q8 and Q9 elements are distinctly different to those associated with the Q4 and Q4X elements. The material distribution results in nonzero local strain variations as shown in Figures 4(b) and (c) respectively.

The local χ fields for the Q8 and Q9 elements, depicted in Figure 4, are recognised as having a significant contribution from higher order straining modes. Recently, Long and Groenwold (2004) have shown that higher order deflection modes of quadratic elements can be softened by employing reduced integration schemes. In the following section, these reduced integration schemes are employed to compute effective material properties of checkerboards with the aim of reducing the strain energy density associated with prescribed strains $\bar{\epsilon}$.

5.2 Effect of element selection and integration scheme on effective properties of a checkerboard

A patch of 4 elements, arranged in a checkerboard as depicted in Figure 2, is used to determine the effect of element formulation and integration scheme on the effective material properties computed using homogenization. In order to compare with results presented by Díaz and Sigmund, their material properties are used. Specifically, the weak material has constitutive tensor

$$E^- = 0, \tag{40}$$

while the strong material has constants

$$E^+_{1111} = E^+_{2222} = 1, E^+_{1122} = 0.3, E^+_{1212} = 0.35. \tag{41}$$

The variable weights selected for evaluation for the 5- and 8-point schemes are based on results presented in Long and Groenwold (2004), wherein it was shown that employing a very small adjustable weight W could result in numerical instabilities, and therefore the use of values $W < 0.01$ are not recommended. Settings of $W_0 = 0.1(8/3)$ and $W_\beta = 0.1(8/9)$ were suggested for improved stability and accuracy. It was also shown that a value of $W_\beta = 40/49$ results in a solution similar to that computed by employing a full 9-point integration scheme for undistorted elements. Values selected for evaluation are therefore $W_0 = 0.01$ and $8/30$ and $W_\beta = 0.01$, $8/90$ and $40/49$.

Effective material properties for the evaluated elements employing the various integration schemes and weights to solve (21) and then (20) are presented in Table 1.

Undistorted Q4 elements are exactly integrated using a 4 point Gauss quadrature, and all other higher order integration schemes therefore yield the same result. The resulting material constants are simply given by the average of the strong and weak material properties since $\epsilon^*[\chi^{(kl)}] = 0$ in (20).

A similar result is computed for the patch of Q4X elements, as expected, since Q4 and Q4X elements result in the same χ fields. The result is that the homogenised material properties of Q4X and Q4 are identical. Furthermore, the integration scheme employed has no effect since the local strains are all constant. Note however, that employing a 4-point scheme results in a rank deficiency for Q4X elements.

Applying a reduced 4-point integration scheme in elemental calculations of Q8 elements is known to result in one spurious straining mode. For an assembly of 2 or more elements, this mode is largely non-communicable. However, as shown in, for example Cook et al (2002); Zienkiewicz and Taylor (1989); Long and Groenwold (2004), the mode becomes communicable under certain circumstances, such as when elements are softly-supported (as may be the case in topology optimization applications), or in some dynamic problems (in which Escher modes appear). In the case considered here, the manner in which

the two solid elements are connected in the patch (similar to a one-node hinge) also allows the mode to become communicable. In other words, the mode is not prevented from propagating between diagonal elements, since adjacent elements are empty.

Solution of the system of equations in (21) under these circumstances is obviously not recommended, due to the rank deficiency of the global stiffness matrix. However, for completeness singularity problems were suppressed in order to compute 'singular results'. Applying the 4-point scheme to the patch of Q8 elements and solving (21) and then (20) results in a constitutive tensor with all non-zero entries equal. This constitutive matrix is therefore rank deficient, and a strain of $\epsilon = \{\bar{\epsilon},\ \bar{\epsilon}, 0\}$ results in zero stress and therefore zero strain energy. This further emphasises that application of the 4-point scheme in a topology optimization environment employing quadratic elements is not recommended.

The 5- and 8-point integration schemes are further evaluated with the weights suggested by Long and Groenwold (2004). The 5-point integration scheme has been shown, even at the low value of adjustable weight ($W_0 = 0.01$), to suppress the spurious mode present when a 4-point scheme is employed. This result is mirrored in the results presented in Table 1. Application of the 8-point scheme, naturally also suppresses communicable modes. As shown in Long and Groenwold (2004), application of the 8-point scheme with weight $W_\beta = 40/49$ yields identical results to a 9-point scheme for undistorted elements.

Identical results are computed when a patch of Q9, instead of Q8, elements are considered. However, application of a 4-point integration scheme to compute the element stiffness matrix of Q9 elements results in 3 spurious zero energy modes, two of which are communicable in an assemblage of elements. As a result, even application of the 5-point scheme results in a rank deficient global stiffness matrix. Therefore, even though the computed results are similar for Q8 and Q9 elements, Q9 elements can only safely be used with 8- or 9-point integration schemes.

Finally, applying a full (9-point) integration scheme results in identical, to machine precision, effective material properties for Q8 and Q9 elements. Since a 9-point scheme represents a full integration scheme for an undistorted quadratic element, the result is identical to solving the expressions analytically. This suggests that there is very little or no advantage in including the hierarchical bubble function, present in Q9 elements, in terms of checkerboarding of undistorted elements. Results for distorted elements may differ however.

5.3 Effect of integration scheme on strain energy density of quadratic elements

Since it was shown in Section 5.2 that both Q4 and Q4X elements result in identical effective material tensors independent of integration scheme, their results are not considered in this section. Results for Q4 elements may be found in the paper of Díaz and Sigmund (1995). Furthermore, since Q8 and Q9 elements produce identical results, as shown in Table 1, only results for Q8 elements will be presented here. Finally, due to the dominance of the SIMP material model in recent years, only results for SIMP will be focused upon in this subsection. However, the results to follow may be extrapolated to other material parameterizations, such as rank 2 materials.

The material parameterization for SIMP is extremely simple, with the equivalent material tensor given by

$$\bar{E}_{\text{SIMP}}(\rho) = \rho^p E^+, \text{ with } p \geq 1. \tag{42}$$

The minimum compliance problems can therefore be written as

$$\max_{\rho^h \in X_M} \min_{u^h \in K^h} \sum_{e=1}^{N} \frac{1}{2} \int_e (\rho^e)^p E^+ \epsilon(u^h) \cdot \epsilon(u^h) \mathrm{d}x - f(u^h), \tag{43}$$

with relevant space of density

$$X_M = \left\{ \rho \in L^\infty(\Omega) :\ 0 \leq \rho \leq 1,\ \int_\Omega \rho \ \mathrm{d}x \leq M \right\}. \tag{44}$$

For the SIMP problem, the strain energy density of a patch with average density ρ can simply be written as

$$w^*_{\text{SIMP}} = \frac{1}{2} (\rho)^p E^+ \bar{\epsilon} \cdot \bar{\epsilon}, \tag{45}$$

for prescribed strain $\bar{\epsilon}$. It can easily be shown that the strain energy density can be written in terms of principal strains as

$$\frac{w^*_{\text{SIMP}}}{E^+_{1111} \epsilon_I^2} = \frac{1}{2} (\rho)^p \left(1 + 2\nu\eta + \eta^2\right), \tag{46}$$

where η is the principal strain ratio $\eta = \frac{\epsilon_{II}}{\epsilon_I}$, with $|\epsilon_I| \geq |\epsilon_{II}|$, the principal strains.

Comparing this result to expressions for the (analytically or fully integrated) strain energy density of a patch of elements, given by

$$\frac{w^*_{Q4}}{E^+_{1111} \epsilon_I^2} = \frac{1}{4} \left(1 + 2\nu\eta + \eta^2\right), \tag{47}$$

for a checkerboard patch of Q4 elements, and

$$\begin{aligned} \frac{w^*_{Q9}}{E^+_{1111} \epsilon_I^2} = & \frac{1}{4} \left[\frac{(47 - 35\nu - 35\nu^2 + 25\nu^3)}{22(6 - 5\nu)} + \right. \\ & \frac{(50 - 26\nu - 70\nu^2 + 50\nu^3)}{22(6 - 5\nu)} \eta + \\ & \left. \frac{(47 - 35\nu - 35\nu^2 + 25\nu^3)}{22(6 - 5\nu)} \eta^2 \right], \end{aligned} \tag{48}$$

for a patch consisting of Q9 elements, Díaz and Sigmund were able to prove the propositions in (33) to (36). They

conject that if w^*_{SIMP} is less than the strain energy density given by the equivalent patch of elements, checkerboarding is likely to occur.

Whereas Díaz and Sigmund compare (46) to equations (47) and (48), we compare the strain energy density given in (46) to the numerically integrated counterparts of (47) and (48), computed with Q8 elements using various numerical integration schemes.

To illustrate, $w^*_{\text{Q8}}(\eta)$, computed using Q8 elements with full (9-point) integration, is plotted for unit E^+_{1111} and ϵ_I and for $\nu = 0.3$ in Figure 6. To reiterate, since Q8 and Q9 elements result in identical effective material properties (see Table 1), the result of w^*_{Q9} is identical and given by (48), assuming the same integration scheme is employed. Also plotted in Figure 6, is $w^*_{\text{SIMP}}(\eta)$ computed using (46) for various values of penalty parameter p and $\rho = 1/2$. Clearly, for values of $1 \leq p < p^*_1$, $w^*_{\text{Q8}}(\eta) < w^*_{\text{SIMP}}(\eta)$, i.e. checkerboarding is unlikely, and when $p \geq p^*_2$, $w^*_{\text{Q8}}(\eta) \geq w^*_{\text{SIMP}}(\eta)$, i.e. checkerboarding is likely to occur (in both cases, independently of η).

For values of $p^*_1 < p < p^*_2$, $w^*_{\text{Q8}}(\eta)$ could be such that $w^*_{\text{Q8}}(\eta) < w^*_{\text{SIMP}}(\eta)$ or $w^*_{\text{Q8}}(\eta) > w^*_{\text{SIMP}}(\eta)$, depending on the strain being experienced. For example, if $p = 3$, $w^*_{\text{Q8}}(\eta) < w^*_{\text{SIMP}}(\eta)$ for $-1 \leq \eta \lessapprox -0.53$ and $w^*_{\text{Q8}}(\eta) > w^*_{\text{SIMP}}(\eta)$ for $-0.53 \lessapprox \eta \leq 1$.

Values of p^*_1 and p^*_2 can similarly be computed for each Poisson's ratio ν and plotted, as shown in Figure 7. Values of p can therefore be selected using this figure so as to minimize the likelihood of checkerboarding. If values of p as large as possible are desired (to penalize intermediate densities), a value of p^*_1 as large as possible is sought. If p^*_1 cannot be altered, the 'next best' would be to increase p^*_2.

Figures 8 and 9 depict the effect of applying the 5-point integration scheme on strain energy density, as a function of principal strain ratio η, for a patch of Q8 elements. The plot is for a material with $\nu = 0.3$, and as before, unit E^+_{1111} and ϵ_I. For clarity, only the 5-point scheme with weights $W_0 = 0.01$ and $W_0 = 8/30$ are depicted, together with the results computed using the 4-point and 9-point schemes for reference.

Clearly, applying the 5-point scheme with $W_0 = 0.01$ or $8/30$ significantly reduces the strain energy density associated with the considered straining modes. It can be shown that there is a monotonic increase in strain energy density with an increase in W_0. In fact, for weights close to the the maximum permitted value, $8/3$, a higher strain energy density is estimated than for the 9-point scheme.

Also shown in Figure 8 are the strain energy densities w^*_{SIMP}, calculated for different values of p. As said, if $w^*_{\text{Q8}}(\bar{\epsilon}) > w^*_{\text{SIMP}}(\bar{\epsilon})$, checkerboarding is likely to occur. Therefore, application of reduced integration schemes clearly reduces the likelihood of checkerboarding for a given p. Alternatively, it allows for the use of larger values of p without increasing the effective stiffness of the checkerboard patch of elements.

Finally, the minimum of w^*_{SIMP} computed using (46) occurs at $\eta = -\nu$, in this case $\eta = -0.3$. Increasing p simply decreases values of w^*_{SIMP}. However, computing the strain energy density of a patch of Q8 elements employing the various integration schemes, affects not only the value of $w^*_{\text{Q8}}(\eta)$, but also shifts the turning point towards $\eta = -1$ as the integration scheme becomes 'softer'. Unfortunately, this means that the gap between p^*_1 and p^*_2 is increased as will be shown in the next subsection.

For clarity, Figure 9 shows an enlargement of Figure 8, concentrating on the lower left corner. As described earlier, applying a 4-point integration scheme (which is equivalent to a 5-point scheme with $W_0 = 0$), results in zero strain energy being experienced at $\eta = -1$, corresponding to the rank deficiency in the constitutive matrix $\bar{E}$. Figure 9 also highlights the difference between the results employing the 4-point scheme and those using the 5-point scheme with $W_0 = 0.01$ and $8/30$, which is not clear in Figure 8.

Figures 10 and 11 depict the results for the same problem employing the 8-point scheme. Again, the results of the 4- and 9-point schemes are plotted together with results for w^*_{SIMP} for various values of p. Employing the 8-point scheme with $W_\beta = 40/49$ clearly produce very similar results to those employing the 9-point scheme as expected. Again, employing low values of W_β (such as 0.01 or $8/90$) produce significantly lower values of strain energy density. Once again, an enlargement of Figure 10 is depicted in Figure 11. Slightly higher values of strain energy density are computed using the 8-point, compared to the 5-point, scheme for low weights, such as 0.01. This is significant, especially since the 5-point scheme is not recommended for Q9 elements.

5.4 Effect of integration scheme on penalty bounds p^*_1 and p^*_2

Comparing the strain energy density for a checkerboard patch of Q8 elements, using the various integration schemes, to the corresponding expression for the SIMP material model in (46), limits on p can be determined for which $w^*_{\text{Q8}}(\bar{\epsilon}) < w^*_{\text{SIMP}}(\bar{\epsilon})$, denoted $p^*_1(\nu)$ and for which $w^*_{\text{Q8}}(\bar{\epsilon}) > w^*_{\text{SIMP}}(\bar{\epsilon})$, denoted $p^*_2(\nu)$. This can be done for each value of Poisson's ratio ν, as graphically depicted in Figure 7.

In Figure 12, the values of $p^*_1(\nu)$ for Q8 elements employing the 5-point scheme are plotted, normalised with respect to the fully integrated equivalent, (shown in Figure 7). Also plotted as a reference are the values computed using 4- and 9-point integration schemes. The figure shows that employing the 5-point scheme with $W_0 = 0.01$ increases p^*_1 significantly, almost to the level of the 4-point scheme. Compared to analytical or full integration, at a Poisson's ratio of $\nu = 0.3$ (common in engineering materials) an increase of approximately 10% is achieved through application of this integration scheme.

A slightly less marked increase is achieved by employing the 5-point scheme with $W_0 = 8/30$.

Figure 13 depicts the results employing the 8-point scheme. In this case, the increase is approximately 10% for both weights $W_\beta = 0.01$ and $W_\beta = 8/90$. Once again, as expected, employing the 8-point scheme with a weight $W_\beta = 40/49$ results in identical trends to the results computed with the 9-point scheme.

Figures 14 and 15 depict the values of $p_2^*(\nu)$ for a patch of Q8 elements employing 5- and 8-point schemes, respectively. It was shown in Section 5.3, that for the 4-point scheme as $\eta \to -1$, $w_{\text{Q8}}^* \to 0$. This implies that $p_2^* \to \infty$. The results for the 4-point scheme are therefore not shown in Figures 14 and 15.

The scale of improvement for p_2^* is considerably higher than that of p_1^*. Improvements of well over 300% for the 5-point scheme using $W_0 = 0.01$ and around 300% for the 8-point scheme with $W_\beta = 0.01$ are achieved. The result is in a relatively wide range of values for p, in for which checkerboarding likelihood depends on strain conditions. However, since reduced integration does not add to element numerical cost (in fact cost is reduced) and accuracy is improved with no loss of stability, as shown in Long and Groenwold (2004), it is recommend that our reduced integration schemes be implemented for topology optimization problems.

6 Conclusions

Based on the theory of Díaz and Sigmund (1995), the stiffness of checkerboard patches of various elements, employing different integration schemes have been assessed. Standard bilinear isoparametric 4-node elements and higher order 8- and 9-node elements, as well as 4-node elements with in-plane rotational degrees of freedom have been evaluated. Full, reduced and modified reduced integration schemes were employed. Combinations of element formulations and integration schemes which 'soften' the effective material properties of a checkerboard, thereby effectively reducing the likelihood of checkerboarding, were sought.

Firstly, when analyzed according to the theory proposed by Díaz and Sigmund (1995), it was shown that both 4-node elements with drilling degrees of freedom (Q4X) and without (Q4) result in identical effective material properties for a checkerboard patch of elements. The additional degrees of freedom present in Q4X elements do not 'soften' the patch since the 3 linearly independent test strains, applied to compute the effective material properties, do not activate the nodal in-plane rotations. It was however numerically demonstrated that for practical problems, where nodal rotations are non-zero, checkerboarding is somewhat reduced. However, since in the limit of mesh refinement only constant strain states are experienced, there is no guarantee that Q4X elements will unconditionally eliminate checkerboarding.

Next, the stiffness of a checkerboard consisting of higher-order elements, evaluated using various reduced integration schemes, were considered. We started by showing that the checkerboard stiffness in a regular mesh consisting of Q8 and Q9 elements is identical, assuming of course that the same numerical integration scheme is employed in elemental calculations.

We then showed that Q8 elements using 5-, 8- or 9-point integration schemes are problem free in terms of rank deficiencies on the elemental level, whereas Q9 elements are only rank sufficient when employing the 8- or 9-point schemes. Although traditionally the 'hourglass' mode present in Q8 elements is said to be non-communicable in an assemblage of two or more elements, the 'black-and-white' checkerboard patch presents a practical example of a situation where this mode can in fact propagate through the mesh. We therefore illustrated that a 4-point reduced integration scheme is, in theory, unsuitable for the evaluation of Q8 or Q9 elements in topology optimization.

Of the evaluated combinations, the most significant improvements in terms of reducing the effective stiffness of a checkerboard, were achieved by employing a 5-point integration scheme (with associated variable weight $W_0 = 0.01$) applied to Q8 elements. When compared to Q9 elements with full integration, employing this combination increases the value of p_1^* by approximately 10%, while p_2^* is increased by over 300% for common engineering materials. Therefore, in principle, a 10% higher value of p can be used without any increased risk of checkerboarding, while a 300% increase in p can be affected before checkerboarding becomes likely, indepedent of the strain state. This benefit is also cost-effective since employing the 5-point scheme simultaneously reduces computational cost on the element level, and increases the accuracy of the finite element approximation.

It is therefore recommended that Q8 elements employing a 5-point integration scheme be used, instead of Q8 elements with a 4- or 9-point scheme, or Q9 elements with full integration, when higher order elements are employed in topology optimization applications using undistorted elements.

References

Allman D (1988) A quadrilateral finite element including vertex rotations for plane elasticity analysis. Int J Numer Meth Engng 26:717–730

Bendsøe M (1989) Optimal shape design as a material distribution problem. Struct Optim 1:193–202

Bendsøe M (1995) Optimization of structural topology, shape, and material. Springer, Berlin

Bendsøe M, Kikuchi N (1988) Generating optimal topologies in structural design using a homogenization method. Comput Methods Appl Mech Engrg 71:197–224

Bendsøe M, Sigmund O (2003) Topology Optimization: Theory, Methods and Applications. Springer, Berlin

Bruns T, Tortorelli D (2001) Topology optimization of nonlinear elastic structures and compliant mechanisms. Comput Methods Appl Mech Engrg 190:3443–3459
Cook R, Malkus D, Plesha M, Witt R (2002) Concepts and applications of finite element analysis. John Wiley and Sons, New York
Díaz A, Kikuchi N (1992) Solutions to shape and topology eigenvalue optimization problems using a homogenization method. Int J Numer Meth Engng 35:1487–1502
Díaz A, Sigmund O (1995) Checkerboard patterns in layout optimization. Struct Optim 10:40–45
Dovey H (1974) Extension of three dimensional analysis to shell structures using the finite element idealization. Report no. UC SESM 74-2, Ph-D dissertation, University of California, Berkeley
Geyer S, Groenwold A (2003) On reduced integration and locking of flat shell finite elements with drilling rotations. Commun Num Meth Eng 19:85–97
Gupta A, Mohraz B (1972) A method of computing numerically integrated stiffness matrices. Int J Numer Meth Engng 5:83–89
Hassani B, Hinton E (1998a) A review of homogenization and topology opimization II-analytical and numerical solution of homogenization equations. Computers and Structures 69:719–738
Hassani B, Hinton E (1998b) A review of homogenization and topology optimization I-homogenization theory for media with periodic structure. Computers and Structures 69:707–717
Hassani B, Hinton E (1998c) A review of homogenization and topology optimization III-topology optimization using optimality criteria. Computers and Structures 69:739–756
Hughes T, Brezzi F (1989) On drilling degrees of freedom. Comput Methods Appl Mech Engrg 72:105–121
Ibrahimbegovic A, Taylor R, Wilson E (1990) A robust quadrilateral membrane finite element with drilling degrees of freedom. Int J Numer Meth Engng 30:445–457
Irons B (1971) Quadrature rules for brick based finite elements. Int J Numer Meth Engng 3:293–294
Jog C, Haber R (1996) Stability of finite element models for distributed-parameter optimization and topology design. Comput Methods Appl Mech Engrg 130:203–226
Jog C, Haber R, Bendsøe M (1993) A displacement-based topology design method with self-adaptive layered materials. In: Bendsøe M, Mota Soares C (eds) Topology Design of Structures, Kluwer Academic Publishers, Dordrecht, The Netherlands
Long C, Groenwold A (2004) Reduced modified quadrature for quadratic membrane finite elements. Int J Num Meth Eng 61:837–855
Long C, Loveday P, Groenwold A (2003) On membrane elements with drilling degrees of freedom in topology optimization. In: Proc. Fifth World Congress on Structural and Multidisciplinary Optimization, Lido di Jesolo, Venice, Italy, paper no. 83
Long C, Groenwold A, Loveday P (2004) Implications of finite element formulation in optimal topology design. In: Zingoni A (ed) Progress in Structural Engineering, Mechanics and Computation, Cape Town, South Africa, pp 1015–1019
Long C, Loveday P, Groenwold A (2005) Design of a piezoelectric mirror scanning device using topology optimization. In: Proc. Sixth World Congress on Structural and Multidisciplinary Optimization, Rio de Janeiro, Brazil, paper no. 4031
Long C, Geyer S, Groenwold A (2006) A numerical study of the effect of penalty parameters for membrane elements with independent rotation fields and penalized equilibrium. Finite Elements in Analysis and Design 42:757–765
Pedersen N (2000) Maximization of eigenvalues using topology optimization. Struct Multidisc Optim 20:2–11
Poulsen T (2002a) A simple scheme to prevent checkerboard patterns and one-node connected hinges in topology optimization. Struct Multidisc Optim 24:396–399
Poulsen T (2002b) Topology optimization in wavelet space. Int J Numer Meth Engng 53:567–582
Sigmund O (1994) Materials with prescribed constitutive parameters: an inverse homogenization problem. International Journal of Solids and Structures 31:2313–2329
Sigmund O (1997) On the design of compliant mechanisms using topology optimization. Mechanics of Structures and Machines 25:495–526
Sigmund O (2001a) Design of multiphysics actuators using topology optimization - Part I: One-material structures. Comput Methods Appl Mech Engrg 190:6577–6604
Sigmund O (2001b) Design of multiphysics actuators using topology optimization - Part II: Two-material structures. Comput Methods Appl Mech Engrg 190:6605–6627
Sigmund O, Petersson J (1998) Numerical instabilities in topology optimization: A survey on procedures dealing with checkerboards, mesh-dependencies and local minima. Struct Multidisc Optim 16:68 – 75
Zhou M, Rozvany G (1991) The COC algorithm, Part II: Topological, geometrical and generalized shape optimization. Comp Meth Appl Mech Engng 89:309–336
Zienkiewicz O, Taylor R (1989) The Finite Element Method, vol I: Basic Formulation and Linear Problems. McGraw-Hill Book Company, London
Zienkiewicz O, Taylor R (1991) The Finite Element Method, vol II: Solid and Fluid Mechanics Dynamics and Nonlinearity. McGraw-Hill Book Company, London
Zienkiewicz O, Taylor R, Too J (1971) Reduced integration techniques in general analysis of plates and shells. Int J Numer Meth Engng 3:275–290

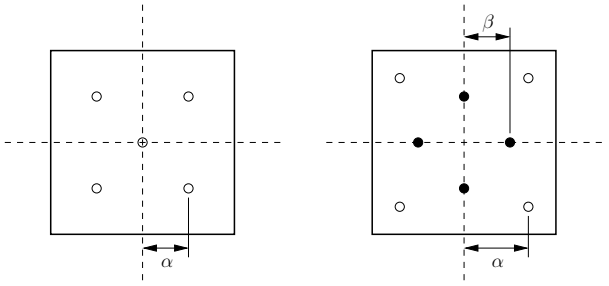

(a) 5-point scheme. (b) 8-point scheme.

Fig. 1 Reduced modified integration schemes.

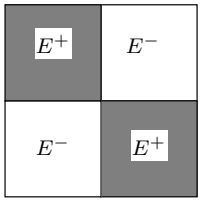

Fig. 2 Checkerboard patch with average density ρ =1/2.

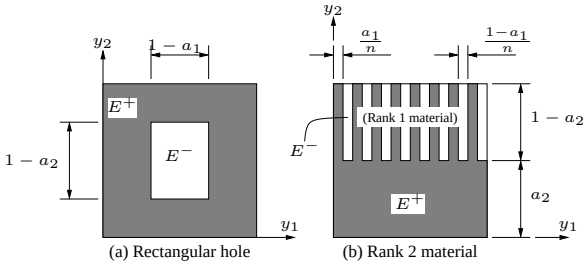

(a) Rectangular hole (b) Rank 2 material

Fig. 3 Example base cells often used in topology optimization.

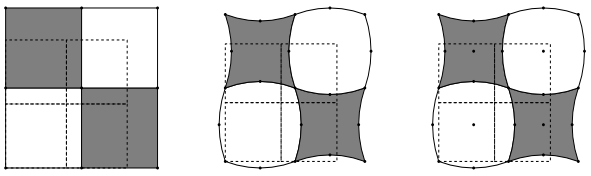

(a) Q4 and Q4X (b) Q8 (c) Q9

Fig. 4 Local χ fields for various elements resulting from mean strain field $\bar{\epsilon}_{11} = \bar{\epsilon}_{22} = 1$ and $\bar{\epsilon}_{12} = 0$.

(a) Q4 elements. (b) Q4X elements

Fig. 5 Optimal topologies of the MBB beam using symmetry and employing (a) Q4 and (b) Q4X elements.

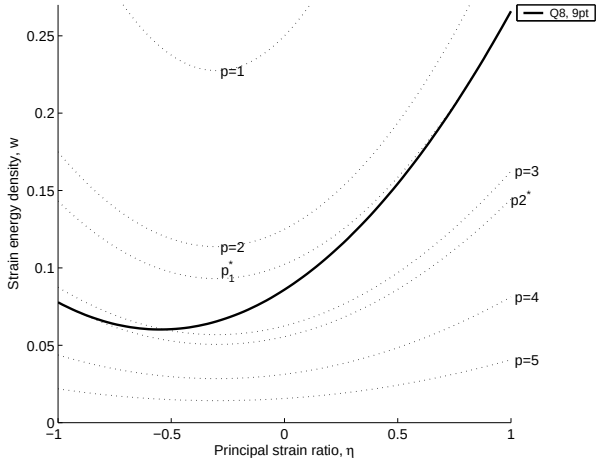

Fig. 6 Strain energy density of fully integrated Q8 elements.

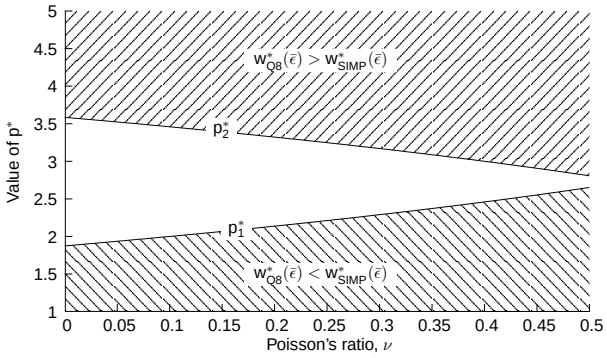

Fig. 7 Variation of p^* for fully integrated Q8 elements.

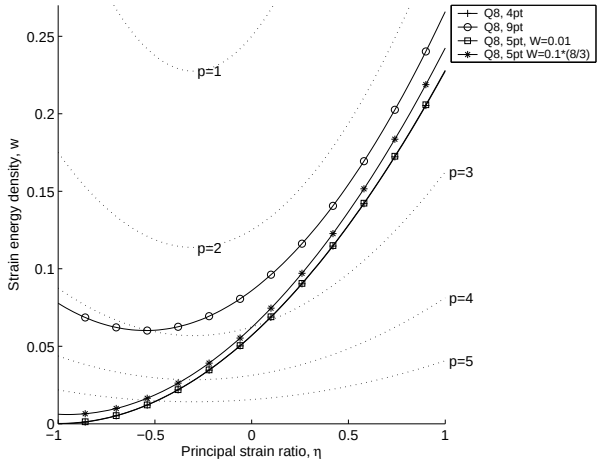

Fig. 8 Strain energy density of Q8 elements with 5-point integration scheme.

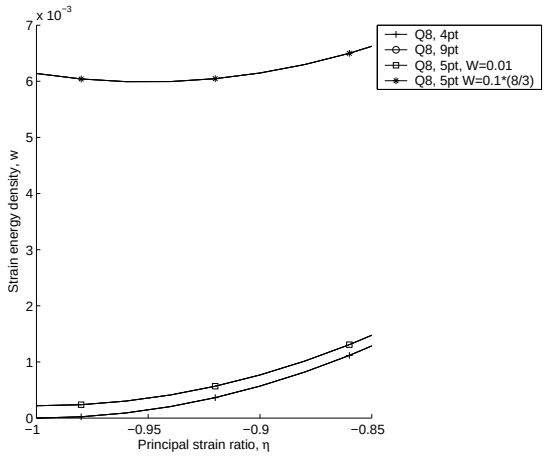

Fig. 9 Strain energy density of Q8 elements with 5-point integration scheme. Zoom of Figure 8.

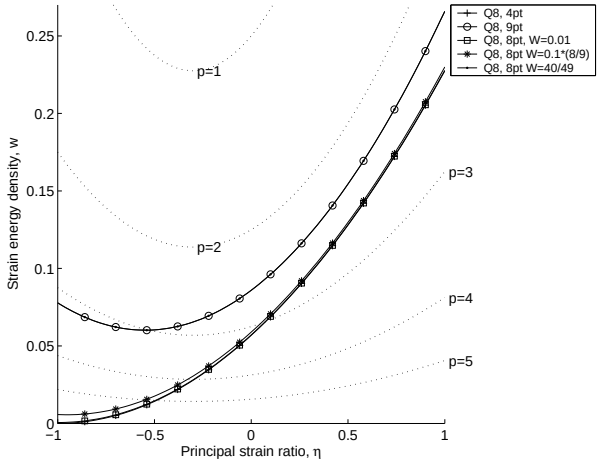

Fig. 10 Strain energy density of Q8 elements with 8-point integration scheme.

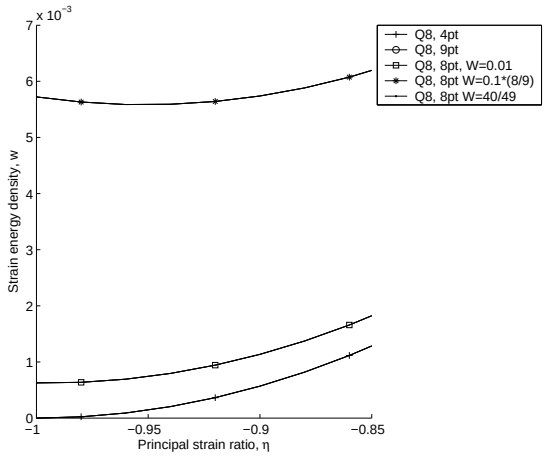

Fig. 11 Strain energy density of Q8 elements with 8-point integration scheme. Zoom of Figure 10.

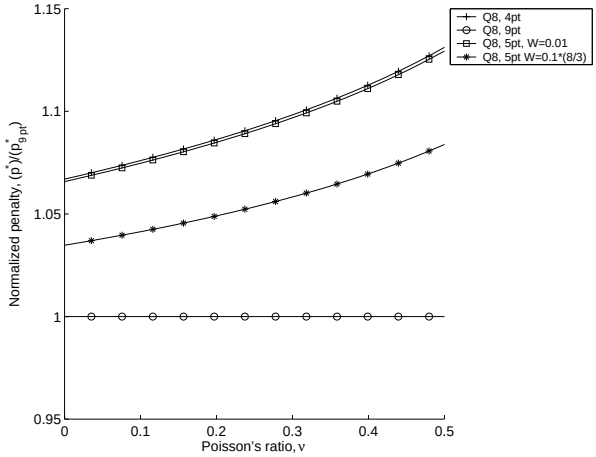

Fig. 12 Effect of integration scheme on p_1^*: 5-point scheme.

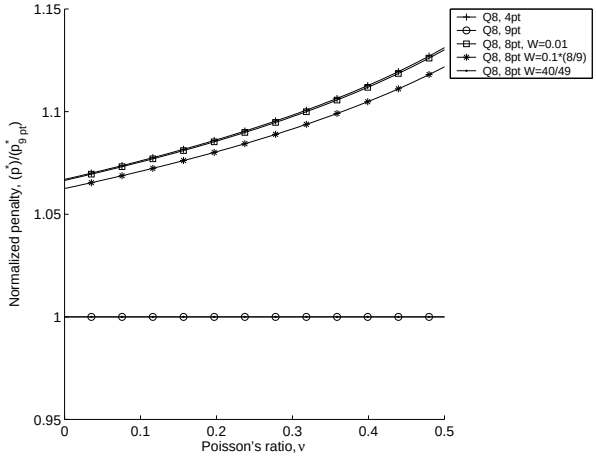

Fig. 13 Effect of integration scheme on p_1^*: 8-point scheme.

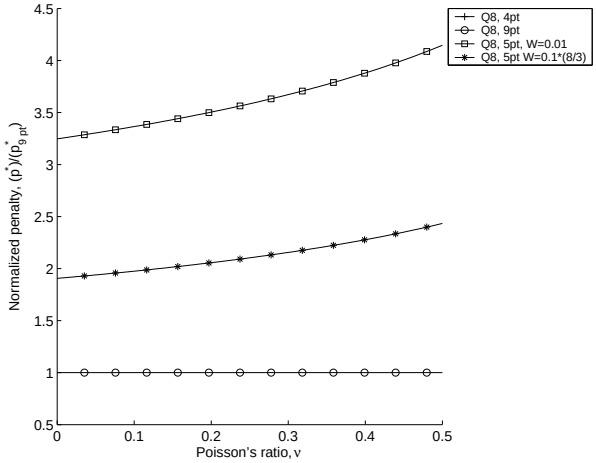

Fig. 14 Effect of integration scheme on p_2^*: 5-point scheme.

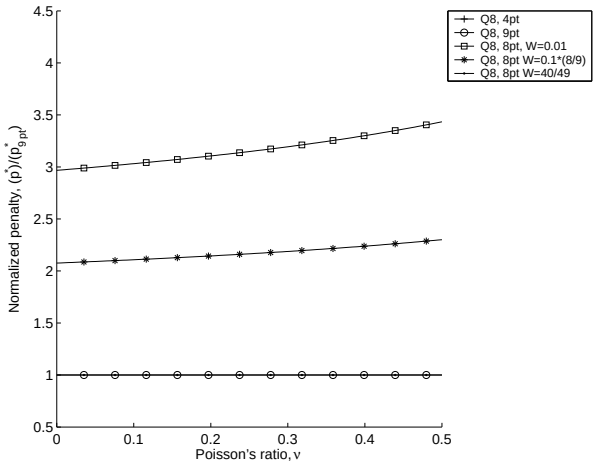

Fig. 15 Effect of integration scheme on p_2^*: 8-point scheme.

Table 1 Effective constitutive terms for different elements employing various integration schemes.

Element	Integration Scheme	Adjustable Weight	$\bar{E}_{1111}$	$\bar{E}_{2211}=$ $\bar{E}_{1122}$	$\bar{E}_{2222}$	$\bar{E}_{1212}$
Q4	4pt	N/A	0.50000	0.15000	0.50000	0.17500
Q4	5pt	Any	0.50000	0.15000	0.50000	0.17500
Q4	8pt	Any	0.50000	0.15000	0.50000	0.17500
Q4	9pt	N/A	0.50000	0.15000	0.50000	0.17500
Q4X	4pt*	N/A	0.50000	0.15000	0.50000	0.17500
Q4X	5pt	Any	0.50000	0.15000	0.50000	0.17500
Q4X	8pt	Any	0.50000	0.15000	0.50000	0.17500
Q4X	9pt	N/A	0.50000	0.15000	0.50000	0.17500
Q8	4pt*	N/A	0.11375	0.11375	0.11375	0.11375
Q8	5pt	$W_0 = 0.01$	0.11413	0.11391	0.11413	0.11386
Q8	5pt	$W_0 = 0.1\frac{8}{3}$	0.12428	0.11814	0.12428	0.11682
Q8	8pt	$W_\beta = 0.01$	0.11420	0.11357	0.11420	0.11376
Q8	8pt	$W_\beta = 0.1\frac{8}{9}$	0.11783	0.11211	0.11783	0.11387
Q8	8pt	$W_\beta = \frac{40}{49}$	0.17184	0.09407	0.17184	0.11582
Q8	9pt	N/A	0.17184	0.09407	0.17184	0.11582
Q9	4pt*	N/A	0.11375	0.11375	0.11375	0.11375
Q9	5pt*	$W_0 = 0.01$	0.11413	0.11391	0.11413	0.11386
Q9	5pt*	$W_0 = 0.1\frac{8}{3}$	0.12428	0.11814	0.12428	0.11682
Q9	8pt	$W_\beta = 0.01$	0.11420	0.11357	0.11420	0.11376
Q9	8pt	$W_\beta = 0.1\frac{8}{9}$	0.11783	0.11211	0.11783	0.11387
Q9	8pt	$W_\beta = \frac{40}{49}$	0.17184	0.09407	0.17184	0.11582
Q9	9pt	N/A	0.17184	0.09407	0.17184	0.11582

* Singularity problems suppressed to perform the calulation.